Chinese Chemical Letters 34 (2023) 108426

Contents lists available at ScienceDirect

Chinese Chemical Letters

journal homepage: www.elsevier.com/locate/cclet

Composite Eu-MOF@CQDs "off & on" ratiometric luminescent probe for highly sensitive chiral detection of L-lysine and 2-methoxybenzaldehyde

Yupeng Jiang, Xinhui Fang, Ziqing Zhang, Xiaomeng Guo, Jianzhong Huo, Qian Wang, Yuanyuan Liu, Xinrui Wang*, Bin Ding*

Tianjin Key Laboratory of Structure and Performance for Functional Molecule, College of Chemistry, Tianjin Normal University, Tianjin 300387, China

ARTICLE INFO

Article history:
Received 28 February 2023
Revised 14 March 2023
Accepted 3 April 2023
Available online 6 April 2023

Keywords:
Photo-luminescence
Carbon quantum dots
Composite material
L-Lysine
2-Methoxybenzaldehyde
Isomers

ABSTRACT

The high amount of L-lysine can increase the potential risk of cardiovascular disease. Additionally, 2-methoxy benzaldehyde (2-MB) has high toxicity and can easily pollute the environment. In this work, carbon quantum dots (CQDs) can be encapsulated into Eu-BTB (H_3BTB = 1,3,5-tri(4-carboxyphenyl)benzene), forming the multi-emission composite material Eu-BTB@CQDs. It has two emissions peaks (617 nm for Eu and 470 nm for CQDs). Eu-BTB@CQDs can be applied as bi-functional ratiometric "off & on" luminescent sensor for L-lysine and 2-MB with high sensitivity and selectivity, the low limit of detection (LOD) for L-lysine is 3.68 μmol/L and for 2-MB is 0.54 μmol/L, respectively. Additionally, Eu-BTB@CQDs can quantitatively discriminate L-lysine in the mixed D- and L-lysine water solutions (five different concentrations ratio of L/D-lysine has been set) makes the chiral detection of L-lysine are more meaningful. On the other hand, Eu-BTB@CQDs also can detect 2-MB over 4-methoxybenzaldehyde (4-MB) with high selectivity. Further the detection of 2-MB and L-lysine in the lake water real samples with the reasonable recovery rate. Finally, the detection mechanisms for L-lysine and 2-MB were also investigated and discussed in detail.

Metal organic framework (MOF) is micro-porous coordination compounds containing diverse metal cations or metal clusters and organic ligands. Due to excellent physical and chemical properties, MOF is widely applied in gas storage [1,2], heterogeneous catalysis [3,4], drug delivery [5,6], and biological imaging [7,8]. The structure and optical properties of MOF can be tuned by using different organic ligands. Therefore, different luminescent MOF can be applied as the detection platform for various analytes such as anions [9], cations [10], amino acids [11], and essential industrial organic molecules [12,13].

Recently, lanthanide metal organic framework (Ln-MOF) possess following excellent performances. Lanthanide ions combined with ligand can form the high stable Ln-MOF and remain stable in an extreme environment. Additionally, lanthanide ions have high coordination numbers, enrich their connectivity with organic ligand with diverse coordinated modes. Given to functional ligand, the low quantum yield due to f-f transition inhibition [14] can be solved by the antenna effect [15]. As a result, lanthanide characteristic luminescence emissions of Ln-MOF was applied to luminescent sensing [16]. In 2017, Ji *et al.* synthesized $Tb(L)(H_2O)_5$ (L = 3,5-dicarboxy-phenol) [17]. This Tb-MOF exhibits an intensive green emission and Pb^{2+} behaves strong quenching effect to Tb-MOF, which can be designed for the quantitative detection of Pb^{2+}. In 2019, Cui *et al.* explored a dual-emission ratiometric luminescent sensor Eu-MOF based on the ligand of 5-boronobenzene-1,3-dicarboxylic acid under solvothermal conditions [18]. Eu-MOF as a luminescent probe that detects glucose and H_2O_2 with good sensitivity and selectivity.

In recent years, researchers have been interested in the synthesis of Ln-MOF by using carboxylic acid ligands with highly conjugated aromatic backbone. Large-scale rigid aromatic frameworks can form stable highly dimensional coordination framework. In 2018, Zhang *et al.* synthesis a 3D framework, namely $[Zn_3(L)_2(bipy)(\mu_3\text{-}OH)_2]\cdot 3H_2O$ (bipy = 4,4′-bipyridine, H_2L = 9*H*-carbazolyl-3,6-dicarboxylic acid). Herein H_2L is a rigid ligand with rich π-electrons, this MOF with a 3D structure can used as a luminescence probe for nitroaromatic compounds detection and Fe^{3+} detection with high sensitivity and can keep stable during detection progress [19]. Recently, porous MOF containing H_3BTB (1,3,5-tri(4-carboxyphenyl)benzene) ligand have been attracted because of their large channels and intriguing properties.

* Corresponding authors.
E-mail addresses: wangxinrui-tjnu@outlook.com (X. Wang), hxxydb@mail.tjnu.edu.cn (B. Ding).

https://doi.org/10.1016/j.cclet.2023.108426
1001-8417/

In 2019, *Ren et al.* synthesis a water-stable Eu-MOF $\{Eu(BTB)DMF\}_n$. It can realize selective detection of sulfamethazine in water with good sensitivity [20]. In 2021, Zhang *et al.* prepared the water-stable Ti-MOF using isopropyl titanate and H_3BTB, namely ZSTU-2, ZSTU-2 showed obvious luminescent quenching for nitroaromatic compounds and it is particularly sensitive to picric acid [21]. Therefore, large porous Ln-MOF have excellent sensing performance and great potential for post-synthetic modification.

Carbon quantum dots (CQDs) are carbon nanomaterial compounds with excellent photoluminescence properties [22–25]. CQDs have intriguing performance such as high chemical stability, long luminescent lifetime and friendly environment. For example, *Chandra et al.* synthesized an eco-friendly CQDs by using citric acid and thiosemicarbaide. These CQDs possess excellent biocompatibility and low cytotoxicity in HeLa cells. It can be used for picric acid detection in the internal environment [26]. At present, the synthesis strategies of CQDs are mainly divided into two categories: Top-down and bottom-up methods [27]. The CQDs used in this work adopt the bottom-up approach, which was obtained from m-phenylenediamine and anhydrous citric acid by solvothermal reaction conditions. This method is easy to operate, fast, cheap, and high yield.

Amino acids are the most basic substances for life activities. Dietary lysine deficiency may affect muscle synthesis, intestinal function, and bone health [28]. Lysine is widely involved in life, it is converted to acetyl coenzyme A, which is involved in carbohydrate metabolism. Lysine can be used as a carnitine and protein synthesis precursor [29]. Therefore, developing the fast and simple sensing platform to carry out lysine detection is meaningful. In 2019, Liu *et al.* synthesized a novel aldehyde and amino-functionalized luminescent MOF, named Cd-TCHO [30]. Cd-TCHO achieved the quantitative detection of L-lysine through enhancement of luminescent intensity, with the low limit of detection (LOD) of 4 μmol/L. Compared with high-performance liquid chromatography, MOF based luminescent sensors have the advantages of low cost, simple operation, and fast detection speed. On the other hand, 2-methoxy benzaldehyde (2-MB) is an intermediate in organic synthesis used in medicine, luminescent dyes, antibacterial agents [31], flame retardants, and organic catalysts [32]. However, 2-MB is toxic, as an intermediate of organic synthesis, 2-MB can lead to serious pollution in the river and 2-MB can irritate the eyes, skin, and mucous membranes. 4-Methoxybenzaldehyde (4-MB) and 2-MB are isomers, while 4-MB is widely used in the formulation of food flavor. As a food additive, 4-MB should not contain 2-MB which may lead to serious food health and safety problems before use, so the selective identification of 2-MB and 4-MB is necessary.

Multiple emissions ratiometric senor has unique advantages. For example, Wang *et al.* designed and synthesized a dual-functional luminescent sensor $[Eu_2(L)_3\cdot(H_2O)_2\cdot(DMF)_2]\cdot 16H_2O$ [33]. The F^- ion can enhance the luminescent intensity of ligand and quench the luminescent intensity of Eu. The colors changing of Eu-MOF from red to chartreuse can be observed by the naked eye under the irradiation of UV light. Multiple luminescent responses result in visible color changes and greatly improve detection sensitivity.

In this work, considering the combination advantage between CQDs and Ln-MOF, CQDs is also successfully introduced into Eu-BTB to construct the multiple emissions composite luminescent probe Eu-BTB@CQDs (Scheme 1). Eu-BTB@CQDs has two emission peaks (470 nm and 617 nm) when excited at 360 nm. Photoluminescence (PL) experiment showed that Eu-BTB@CQDs can be applied as bi-functional ratiometric "off & on" luminescent sensor for L-lysine and 2-MB with high sensitivity and selectivity (Scheme 2). In addition, when different molar ratios of L-lysine and D-lysine were used in the analytical objects, the linear relationship between

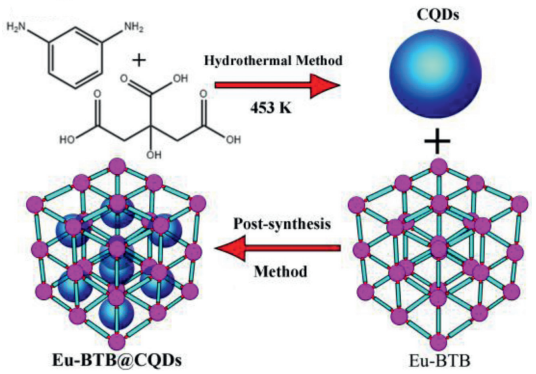

Scheme 1. Preparation of CQDs and Eu-BTB@CQDs.

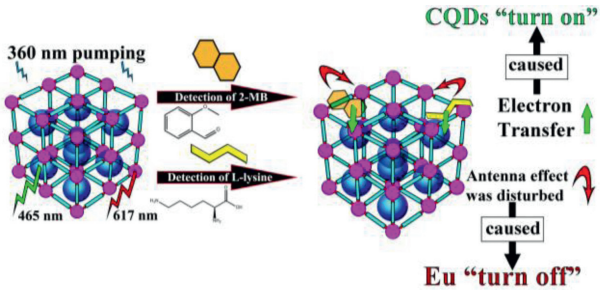

Scheme 2. Composite Eu-BTB@CQDs applied as "off & on" ratiometric luminescent probe for highly sensitive detection of L-lysine and 2-methoxybenzaldehyde.

detection parameter *K* constants and molar amount of L-lysine can be found quantitatively discriminate chiral L-lysine from D-lysine based on Eu-BTB@CQDs. On the other hand, Eu-BTB@CQDs can detect the MB isomers 2-MB and 4-MB. Further, detection mechanisms for L-lysine and 2-MB were also investigated and discussed in detail.

H_3BTB is purchased from ShangHai D&B Biological Science and Technology Co., Ltd. All the other reagents were purchased commercially and used without further purification. Deionized water was used as a solvent in this work. Powder X-ray diffraction (PXRD) was characterized by a D/Max-2500 X-ray diffractometer using Cu-Kα radiation. Fourier transform infrared (FT-IR) spectra (4000–500 cm^{-1}) were recorded by using the NICOLET 6700 FT-IR spectroscope with KBr pellets (NICOLET, USA). Ultrasonic preparation was carried by the SB-100DT Ultrasonic bath (XJ Biotechnology Instrument, Zhejiang, China). PerkinElmer Lambda 35 spectrophotometer was used to determine ultraviolet-visible (UV–vis) adsorption spectra. PL emission spectra were recorded on an RF-5301 spectrophotometer (Daojin, Japan). PL lifetime tests were performed by Fluorolog-3, Horiba Jobin Yvon (USA). Morphology and size of Eu-BTB@CQDs were characterized by Tecnai G^2 F20 transmission electron microscope (TEM; FEI instrument, USA).

Eu-BTB was synthesized according to the method previously reported [34]. Typically, a mixture of $EuCl_3\cdot 6H_2O$ (0.0834 g, 0.2277 mmol) and H_3BTB (0.1 g, 0.2281 mmol) was added into 2.5 mL distilled water, 0.2 mL of NaOH (2 mol/L) solution and 2.5 mL cyclohexanol in a 25 mL Teflon-lined steel autoclave. After the mixture is stirred, the mixture was placed in an oven, heated to 473 K and kept at this temperature for one day. Then the resulting mixture was slowly cooled to room temperature during one day. The resulting product was washed with ethanol three times to get rid of the excess reactants. Finally, white powders were obtained, the yield is 64% (based on H_3BTB ligand).

CQDs was synthesized according to the method previously reported [35]. A mixture of *m*-phenylenediamine (0.05 g,

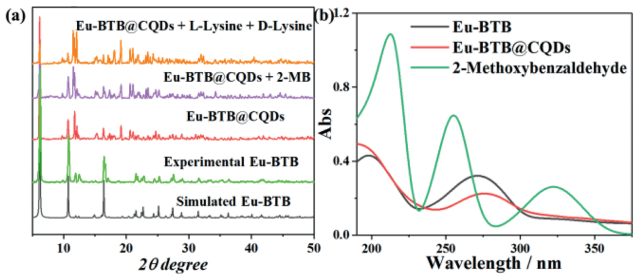

Fig. 1. (a) PXRD patterns of Eu-BTB and Eu-BTB@CQDs in different conditions; (b) UV–vis spectra of Eu-BTB, Eu-BTB@CQDs and 2-methoxybenzaldehyde in the water solutions.

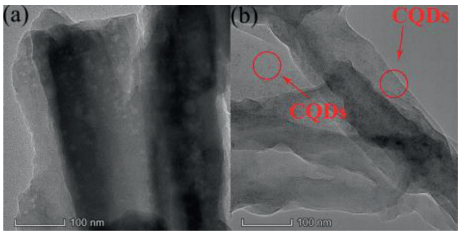

Fig. 2. TEM images of (a) Eu-BTB and (b) Eu-BTB@CQDs.

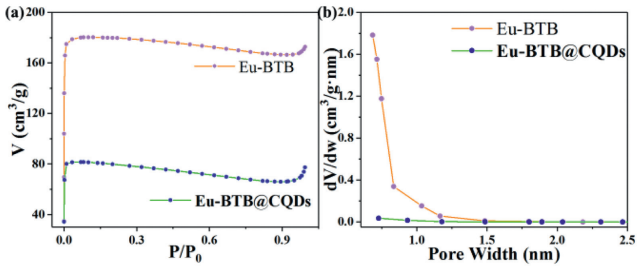

Fig. 3. (a) Nitrogen gas adsorption isotherm at 77 K for Eu-BTB and Eu-BTB@CQDs. (b) Pore distribution for Eu-BTB and Eu-BTB@CQDs.

0.4624 mmol) and anhydrous citric acid (0.088 g, 0.458 mmol) was added into 5 mL distilled water and 5 mL ethanol in a 25 mL Teflon-lined steel autoclave. The mixture was stirred and placed in an oven, heated to 453 K and kept at this temperature for 12 h then cool to room temperature. The product of the reaction filtered by a 200 nm filter membrane, which can retain the supernatant. Finally, the liquid is put in a dialysis membrane (molecular weight cut off is 1000 Da), then dialysis was performed with distilled water for two days with magnetic stirring. After the dialysis process was completed, clear brown CQDs solution outside the dialysis membrane was obtained.

Eu-BTB@CQDs was synthesized by the stirred method constantly at room temperature. Eu-BTB (0.02 g) and CQDs solution (10 mL) were added into a 25 mL beaker, the mixture was stirred continuously for one day. The mixture was centrifuged to remove the supernatant, washed the excess CQDs solution from the precipitate with ethanol. The brown powders Eu-BTB@CQDs were obtained after drying, yield is 82% (based on Eu-BTB).

The concentration of Eu-BTB@CQDs suspension was 0.1 g/L. In the luminescent spectrum experiment, the size of the cuvette was 1 mL, the wavelength of the excitation source is 360 nm and slit is 5 nm.

Crystal description of Eu-BTB is listed in Fig. S1 (Supporting information). PXRD patterns of Eu-BTB are well consistent with experimental ones (Fig. 1a), which demonstrated the purity of as-synthesized Eu-BTB samples [36–39]. Eu-BTB@CQDs immersed in L-lysine and 2-MB solutions are well consistent with theoretical PXRD patterns, which also demonstrated the framework structure of Eu-BTB@CQDs remained stable in the detection process of L-lysine and 2-MB, therefore ratiometric "off & on" luminescent detection process does not cause the structural collapse of Eu-BTB@CQDs.

In the FT-IR spectra, FT-IR bands of Eu-BTB@CQDs can compare with that of Eu-BTB and free H_3BTB, the stretching vibration peak of carbonyl groups located at the position of 1750 cm^{-1} moved to lower wavelength number (Fig. S2 in Supporting information), which also can be attributed to carboxylate groups of H_3BTB coordinated with Eu^{3+} [40–44]. In Fig. S3 (Supporting information), the peak at 1729 cm^{-1} is the stretching vibration peak of the carboxyl group in citric acid (red line). The absorption peak at 1604 cm^{-1} is the bending vibration peak of the amino group in *m*-phenylenediamine (black line). The peak of CQDs at 1650 cm^{-1} is the stretching vibration peak of amide group [45–47]. This shows that the structure of CQDs contains carboxyl and amino groups, in which the carboxyl group in citric acid and amino group in *m*-phenylenediamine have condensation reaction. In the UV–vis spectrum (Fig. 1b), both Eu-BTB and Eu-BTB@CQDs have the absorbed peak located at 275 nm, which should originate from BTB^{3-}. 2-MB has three absorbed peaks at 231, 254 and 324 nm, which can partially overlap with the adsorption of Eu-BTB [48–51]

In TEM image (Fig. 2a), Eu-BTB has the porous structure, and the average particle size of CQDs is not more than 2 nm (Figs. S4a and b in Supporting information). In Eu-BTB@CQDs (Fig. 2b), CQDs located in the pores of Eu-BTB can be observed [52–54]. Luminescent properties of Eu-BTB@CQDs in the water solution are also investigated (Fig. S5 in Supporting information), three emissions located at 364, 470 and 617 nm can be observed, the peak located at 364 nm can be ascribed to H_3BTB ligand emission, the peak located at 470 nm can be attributed to CQDs emission, the peak located at 617 nm can be ascribed to typical Eu^{3+} emission in Eu-BTB emission ($^5D_0 \rightarrow {}^7F_J$) [55–57].

Nitrogen absorption tests for Eu-BTB and Eu-BTB@CQDs were performed (Fig. 3). It is worth noting that there exists significant difference between Eu-BTB and Eu-BTB@CQDs in the nitrogen gas adsorption experiment. The surface area of Eu-BTB is 782.69 m^2/g. This surface area is consistent with previously reported work (MIL-103, BET surface area around 700 m^2/g) [58]. MIL-103 (Ln) is $Ln(C_{27}H_{15}O_6)(H_2O)\cdot(solv)_x$ (Ln = La, Ce, Pr, Nd, Sm, Eu, Gd, Tb, Dy, Ho and Y, solv = H_2O, cyclohexanol). After the introduction of CQDs, the surface area of Eu-BTB@CQDs has been decreased to 355.45 m^2/g, indicating that CQDs can be successfully introduced into the pores of the Eu-BTB [59–61].

Luminescent properties of **E**u-BTB@CQDs were investigated with different amino acid aqueous solutions. Experimental results (Fig. 4a) indicate the emission peak located at 617 nm was obviously quenched with the addition of L-lysine (30 μmol/L), while the emission peak intensity located at 471 nm was simultaneously obviously enhanced (excited at 360 nm and slit is 5 nm). It is noted that other amino acids in water solution do not affect the luminescent emission at 471 nm of Eu-BTB@CQDs, which identify that Eu-BTB@CQDs can selectively discriminate L-lysine (Fig. 4b).

To realize the qualitative detection of L-lysine, Eu-BTB@CQDs suspension is titrated with L-lysine. In Fig. 5a, when the additional amount of L-lysine gradually increased in the concentration range (0–20 μmol/L), the luminescent emission intensity located at 617 nm gradually decreased, while the luminescent emission intensity located at 471 nm gradually increased (excited at 360 nm and slit is 5 nm). To explore the relationship between the concentration of L-lysine and luminescent intensity ratio of Eu-BTB@CQDs, the following equation is used: $I_{471\ nm}/I_{617\ nm} = 15.6422C + 0.8031$ ($R^2 = 0.9927$) (Fig. 5b), the de-

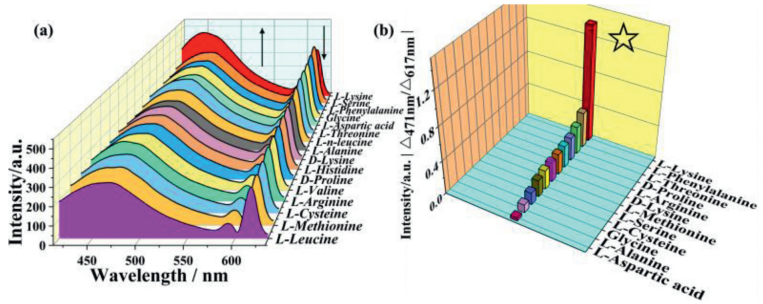

Fig. 4. (a) Luminescent emission spectra of Eu-BTB@CQDs suspension (0.1 g/L, 1 mL) by the addition of different amino acids solutions (30 μmol/L) when excited at 360 nm. (b) The ratio of luminescent intensities ($\triangle_{467\ nm}/\triangle_{617\ nm}$) when different amino acids solutions (30 μmol/L) were added into Eu-BTB@CQDs suspensions (0.1 g/L), respectively (excited position is 360 nm).

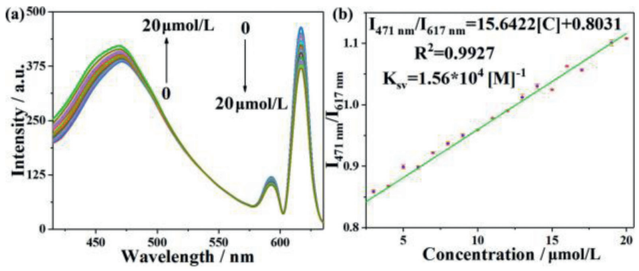

Fig. 5. (a) Luminescent spectra of the Eu-BTB@CQDs (0.1 g/L) with the addition of L-lysine in different concentrations (0–20 μmol/L) when excited at 360 nm, the slit is 5 nm. (b) The linear relationship between luminescent intensity ratio of Eu-BTB@CQDs and the concentration of L-lysine.

tection concentration range is 0–20 μmol/L, the detection sensitivity parameter K (L/mol) is calculated to be 1.56×10^4 L/mol, and low detection limit ($LOD = 3\sigma/K$, σ is the standard deviation of the blank measurement) is 3.68 μmol/L. Further the detection strategy of L-lysine was also applied in the water sample (Table S4 in Supporting information), the recovery rate can be found between 98.71% and 103.35% and the standard deviation (RSD) is less than 2.86%.

To compare with the sensitivity of Eu-BTB@CQDs, Eu-BTB, and CQDs are also used to conduct a quantitative detection on L-lysine (Figs. S6 and S7 in Supporting information). When L-lysine is titrated into Eu-BTB, the luminescent intensity of Eu-BTB (617 nm) continuously decrease with the addition of L-lysine in different concentration (0–20 μmol/L). The following equation is used: $(I_0 - I)/I_0 = 13.6402C + 0.2851$ ($R^2 = 0.8553$, $K = 1.36 \times 10^4$ L/mol). In addition, when L-lysine is titrated into CQDs, the luminescent intensity of CQDs (465 nm) continuously increases with the addition of L-lysine in different concentration (0–20 μmol/L), the following equation is used: $I_0/I = 7.1488C + 1.0010$ ($R^2 = 0.9849$, $K = 7.15 \times 10^3$ L/mol). Compared with Eu-BTB and CQDs, the K value of Eu-BTB@CQDs is higher than that of Eu-BTB and CQDs, respectively. Additionally considering the "off & on" ratiometric detection can avoid more external interference, therefore composite material Eu-BTB@CQDs showed its superiority in quantitative detection of L-lysine.

In addition, Eu-BTB@CQDs has excellent chiral recognition ability for chiral L-lysine and D-lysine. When a series of mixed lysine solutions (the total concentration of the mixed L-lysine and D-lysine is 1 mmol/L) were prepared. Eu-BTB@CQDs is gradually titrated with lysine solutions (Figs. S10-S15 in Supporting information), and a series of detection parameters K values based on the linear fitting equation can be obtained (Fig. S16 in Supporting information). It is noted that K and C (the concentration of L-lysine in the mixed solutions) can obtain a linear relationship, which is represent by: $K = 11774C + 3753$ ($R^2 = 0.9694$). It helps us realize to discriminate chiral L-lysine based on Eu-BTB@CQDs sensing platform. The luminescent properties of L-lysine and D-lysine were different, since D-lysine could not enhance the emission of CQDs obviously (Fig. S15a), which make that Eu-BTB@CQDs can be used for the chiral recognition of L-lysine.

Luminescent properties of Eu-BTB@CQDs were also investigated with different aldehydes aqueous solutions. The experimental results (Fig. 6a) indicated the peak located at 617 nm was obviously quenched by the addition of 2-MB aldehydes solution (24.6 μmol/L), other aldehydes in the water solution do not obviously affect the luminescent emission of Eu-BTB, only 2-MB enhanced the luminescent intensity of CQDs (excited at 360 nm and slit is 5 nm), which showed the superiority recognition of 2-MB by Eu-BTB@CQDs (Fig. 6b). It is important to note that 4-MB (a type of food additive) is an isomer of 2-MB (a chemical raw material), however Eu-BTB@CQDs has no luminescent response to 4-MB. This indicates that if 4-MB contains a small amount of 2-MB, Eu-

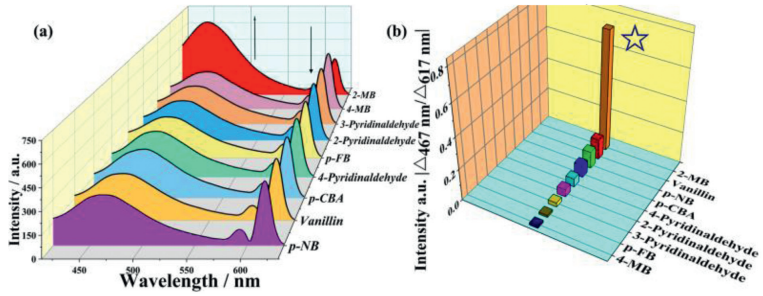

Fig. 6. (a) Luminescent emission spectra of Eu-BTB@CQDs suspension (0.1 g/L, 1 mL) by the addition of different aldehydes solutions (24.6 μmol/L) when excited at 360 nm. (b) The ratio of luminescent intensity difference ($\triangle_{467nm}/\triangle_{617\ nm}$) when different aldehydes solutions (24.6 μmol/L) are added into Eu-BTB@CQDs suspensions (0.1 g/L), respectively (excited position is 360 nm).

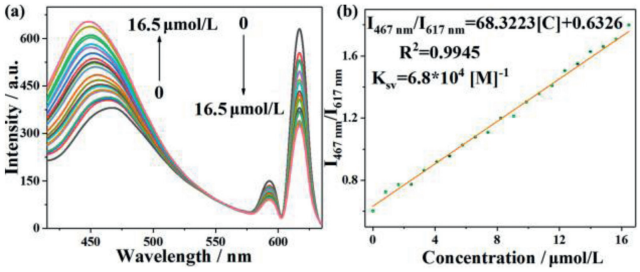

Fig. 7. (a) Luminescent spectra of the Eu-BTB@CQDs (0.1 g/L) with the addition of 2-methoxybenzaldehyde in different concentration (0–16.5 μmol/L), the excited position is 360 nm, the slit is 5 nm. (b) The linear relationship between luminescent intensity ratio of Eu-BTB@CQDs and the concentration of 2-methoxybenzaldehyde.

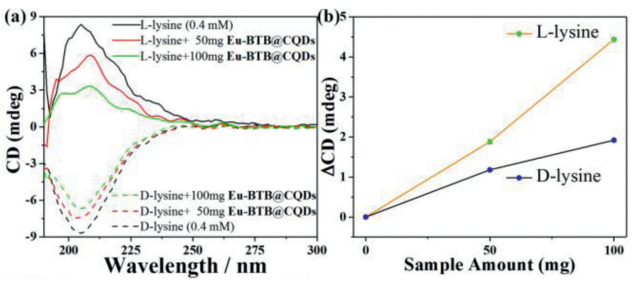

Fig. 8. (a) The CD spectra of L/D-lysine solutions (0.4 mmol/L) with different amounts of Eu-BTB@CQDs added. (b) The ΔCD values of L/D-lysine solutions.

BTB@CQDs can detect 2-MB immediately, which is very meaningful for preventing food safety issues.

In order to realize qualitative detection of 2-MB, Eu-BTB@CQDs suspension is titrated with 2-MB water solution. In Fig. 7a, when 2-MB is gradually added, the concentration of 2-MB increase in the range (0–16.5 μmol/L), it is noted that luminescent emission intensity located at 617 nm gradually decreased, while the luminescent emission intensity for CQDs located at 467 nm was gradually increased (excited at 360 nm and slit is 5 nm). In order to explore the relationship between concentration of 2-MB and luminescent intensity ration of Eu-BTB@CQDs, which using the following equation: $I_{467\ nm}/I_{617\ nm} = 68.3223C + 0.6326$ ($R^2 = 0.9945$) (Fig. 7b), the K is 6.83×10^4 L/mol and LOD is 0.54 μmol/L. Further the detection strategy of 2-MB was also applied in the real lake water sample (Table S5 in Supporting information), the recovery rate can be found between 95.75% and 104.57% and the RSD is less than 4.49%.

In order to compare with the detection sensitivity of Eu-BTB@CQDs, Eu-BTB and CQDs are also used to conduct the quantitative detection of 2-MB, respectively (Figs. S8 and S9 in Supporting information). 2-MB is titrated into Eu-BTB, the luminescent intensity of Eu-BTB (617 nm) was continuously decreased with the addition of 2-MB in different concentration (0–16.5 μmol/L). The following equation is also used: $(I_0 - I)/I_0 = 2.8932C + 0.0698$ ($R^2 = 0.9340$, $K = 2.89 \times 10^4$ L/mol). In addition, 2-MB is also titrated into CQDs, the luminescent intensity of CQDs (465 nm) continuously increased with the addition of 2-MB in different concentration (0–16.5 μmol/L), the following equation is also used: $I_0/I = 1.7646C + 1.0345$ ($R^2 = 0.9964$, $K = 1.76 \times 10^4$ L/mol). Compared with Eu-BTB and CQDs, the K value of Eu-BTB@CQDs is higher than that of Eu-BTB and CQDs, respectively. Additionally, the "off & on" ratiometric Luminescent Probe can avoid more external interference [62–64]. Therefore, the composite material Eu-BTB@CQDs showed its superiority in quantitatively detecting 2-MB.

In order to understand the detection mechanism, the luminescent lifetime of Eu-BTB, CQDs and Eu-BTB@CQDs is also investigated. PXRD result showed that Eu-BTB@CQDs can keep its structure stability in the detection process of L-lysine and the luminescent quenching is not caused by structural collapse Eu-BTB@CQDs.

In the detection process of L-lysine, when CQDs was mixed with L-lysine, the bending vibration peak of amino at 1580 cm^{-1} disappeared (Fig. S17 in Supporting information), and the stretching vibration peak of amide at 1635 cm^{-1} appeared. It also reveals that with the addition of L-lysine, the carboxyl group in CQDs can combine with the amino group in L-lysine, therefore amino group acts as an electron donor group, resulting that the emission of CQDs are significantly enhanced [65–69]. In previous reports, some examples of enhanced luminescent emission due to the introduction of electron-donating groups can be found [70]. In 2020, Al-MIL-53-NO_2 was synthesized by Wang *et al.* This MOF is used to detect H_2S in solutions. In the presence of H_2S, the electron-withdrawing nitro group of the MOF is reduced to the electron-giving amino group, resulting in a significant emission enhancement. On the other hand, when different molar ratio of L-lysine and D-lysine were used in the analytical objects, the linear relationship between detection constants K and molar amount of L-lysine can be found, which can quantitatively discriminate chiral L-lysine from D-lysine based on Eu-BTB@CQDs. In order to explore the binding ability of the Eu-BTB@CQDs to L/D-lysine, we did circular dichroism experiment (Fig. 8a). Under the same concentration of L/D-lysine, after adding different amount of Eu-BTB@CQDs the change of $\Delta CD_{(L\text{-lysine})}$ in L-lysine solution is more significant than $\Delta CD_{(D\text{-lysine})}$ in D-lyisne (Fig. 8b). This indicated that Eu-BTB@CQDs has a stronger binding ability with L-lysine than D-lysine. The active sites of Eu-BTB@CQDs are more likely to bind to L-lysine than D-lysine. L-Lysine can occupy more active sites, and enhance the emission of CQDs through electron transfer mechanism. That is the reason why Eu-BTB@CQDs is more sensitive to L-lysine detection than D-lysine. Different steric hindrances of L-lysine and D-lysine towards to Eu-BTB@CQDs in the electron transfer process may play the important role [71].

In addition, luminescent lifetime parameters are important for judging the detection mechanism [72,73]. According to the average lifetime parameters, we can determine whether the energy transfer process exists. According to the position of initial point, we can determine the pattern of quenching (static quenching or dynamic quenching) [74,75]. The lifetime at 617 nm was excited by 360 nm, and slit is 12 nm, the lifetime at 364 nm was excited by 295 nm, and slit is 12 nm. The luminescent lifetime of Eu-BTB at 617 nm is 3.4094 ns (Fig. S19 and Table S1 in Supporting information). In the Eu-BTB@CQDs, luminescent lifetime at the position of 617 nm been increased to 7.8947 ns, which identify the energy transfer process between Eu-BTB and CQDs. Then, the lifetime of Eu-BTB@CQDs solution (0.1 g/L) with the addition of L-lysine is also investigated. With the concentration of L-lysine increased (0–100 μmol/L), the luminescent lifetime of H_3BTB located at 364 nm decreased from 23.40 ns to 22.74 ns (Fig. 9a and Table S2 in Supporting information), meanwhile, the luminescent lifetime located at 617 nm decreased from 7.89 ns to 7.46 ns (Fig. 9b), which should be correlated with quenching phenomena of Eu-BTB emission peak at the position of 617 nm. This can prove that the antenna effect between H_3BTB and Eu^{3+} was interfered by the addition of L-lysine, which reduces the energy transfer from H_3BTB to Eu^{3+}. As a result, the electron transfer (electron-donating and electron-withdrawing groups) and the interruption of antenna effect (H_3BTB and central Eu) should be important in the detection process of L-lysine.

PXRD results showed that Eu-BTB@CQDs could keep its structural stability in the detection process of 2-MB. 2-MB does not cause the collapse of the framework structure Eu-BTB@CQDs. As for FT-IR of 2-MB (Fig. S18 in Supporting information), when CQDs was mixed with 2-MB, the stretching vibration peak of aromatic

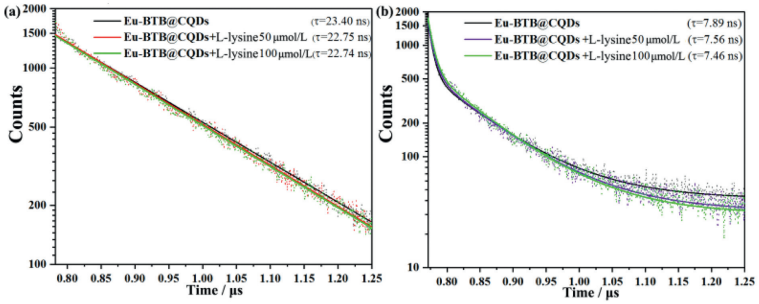

Fig. 9. (a) Luminescent lifetime of the Eu-BTB@CQDs with the addition of L-lysine in different concentration (0–100 μmol/L) at 364 nm, which excited at 295 nm. (b) Luminescent lifetime of the Eu-BTB@CQDs band located at 617 nm with the addition of L-lysine in different concentration (0–100 μmol/L) which excited at 360 nm.

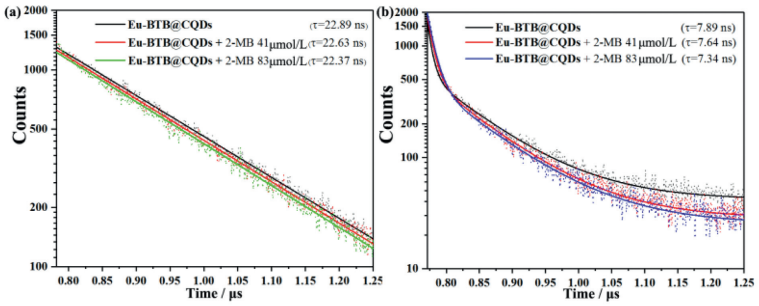

Fig. 10. (a) The luminescent lifetime of the Eu-BTB@CQDs with the addition of 2-MB in different concentration (0–83 μmol/L) at 364 nm which excited at 295 nm. (b) Luminescent lifetime of the Eu-BTB@CQDs with the addition of 2-MB in different concentration (0–83 μmol/L) at 617 nm, which excited at 360 nm.

C=N appeared at 1481 cm^{-1}. It proves that with the addition of 2-MB, the amino group in the CQDs structure can react with the aldehyde group in the 2-MB structure to form schiff base so that 2-MB acts as an electron donor group, resulting that the emission of CQDs of Eu-BTB@CQDs are significantly enhanced [76,77].

To reason why that 2-MB behaved with stronger sensing performance to Eu-BTB@CQDs than 4-MB, steric hindrances play the essential role. Experimental results (Fig. S20 in Supporting information) show that with the increase of steric hindrance of the substituent group (-OMe, -OEt, -O-*n*-Pr), these 2-MB isomers approached more difficulty to Eu-BTB@CQDs, which leads to the obstruction of the enhancement process of CQDs emission and the *K* value decline gradually (Figs. S21 and S22 in Supporting information), which identify different steric hindrances caused by different position isomers should be important for the electron transfer between Eu-BTB@CQDs and 2-MB [78]. This steric hindrance-based luminescent sensing mechanism can greatly improve these target objects' detection efficiency and selectivity [79]. For example, in 2021, Lee *et al.* synthesis a Tb-benzenetricarboxylate (BTC) metal-organic framework, namely Tb-BTC MOF. Tb-BTC MOF can be used for organic amines detection (such as ethylenediamine, diethanolamine, diethylamine) through fluorescence quenching of Tb emission. The quenching efficiency of the amine solutions relied on the steric hindrance between the analytes and MOF [80].

Luminescent lifetime parameters are also crucial for detection mechanism analysis [81,82]. The lifetime at 617 nm was excited by 360 nm, and the slit is 12 nm, the lifetime at 364 nm was excited by 295 nm, and the slit was 12 nm. The lifetime of Eu-BTB@CQDs solution (0.1 g/L) with the addition of 2-MB is also investigated. When concentration of 2-MB increases (0–83 μmol/L), the lifetime of H_3BTB at the position of 364 nm has been decreased from 22.89 ns to 22.37 ns (Fig. 10a and Table S3 in Supporting information). Meanwhile, when the concentration of 2-MB increases from 0 to 83 μmol/L, luminescent lifetime at the position of 617 nm decreases from 7.89 ns to 7.34 ns (Fig. 10b), which demonstrates that the energy transfer from H_3BTB to 2-MB, the antenna effect between H_3BTB and Eu^{3+} is also weakened in the detection process of 2-MB. Therefore, the mechanism of the detection process of 2-MB and L-lysine may be similar. Electron transfer and interfere of antenna effect plays a major role in the detection process of 2-MB.

In conclusion, multi-emission composite "off & on" ratiometric luminescent probe Eu-BTB@CQDs was synthesized by post-synthesized method, which has been characterized by PXRD, FT-IR, UV–vis spectrum, TEM and luminescent spectrum. CQDs can be encapsulated into Eu-BTB, forming the composite dual-emission sensor. It can not only maximize the advantages of CQDs using the cheap raw material, simple synthesis method, and low biological toxicity, but also improve the disadvantage of CQDs single emission which leads to the vulnerability of luminescent detection for background interference. Eu-BTB@CQDs can provide the novel method and platform for conducting simple, sensitive and efficient luminescent detection of L-lysine and 2-MB. As a result, these MOF@CQDs composite materials have great potential to be developed for a wider range of functions and applications in luminescent sensing detection. Chiral discrimination and isomer discrimination are of great significance for medical medicine, chemical production, food safety and other fields. This work can serve as the excellence sensing platform for the follow-up research, which is helpful to design more luminescent sensors for industrial and life production in the future.

Declaration of competing interest

The authors declare that they have no known competing financial interests or personal relationships that could have appeared to influence the work reported in this paper.

Acknowledgment

This work was supported financially by Science &Technology Development Fund of Tianjin Education Commission for Higher Education (No. 2019ZD15).

Supplementary materials

Supplementary material associated with this article can be found, in the online version, at doi:10.1016/j.cclet.2023.108426.

References

[1] J.R. Li, R.J. Kuppler, H.C. Zhou, Chem. Soc. Rev. 38 (2009) 1477–1504.
[2] H. Furukawa, N. Ko, Y.B. Go, et al., Science 329 (2010) 424–428.
[3] J.W. Liu, L.F. Chen, H. Cui, et al., Chem. Soc. Rev. 43 (2014) 6011–6061.
[4] Y.B. Huang, J. Liang, X.S. Wang, R. Cao, Chem. Soc. Rev. 46 (2017) 126–157.
[5] M.X. Wu, Y.W. Yang, Adv. Mater. 29 (2017) 1–20.
[6] J.Y. An, S.J. Geib, N.L. Rosi, J. Am. Chem. Soc. 131 (2009) 8376–8377.
[7] D.M. Liu, K.D. Lu, C. Poon, W.B. Lin, Inorg. Chem. 53 (2014) 1916–1924.
[8] A. Foucault-Collet, K.A. Gogick, K.A. White, et al., Proc. Natl. Acad. Sci. U. S. A. 110 (2013) 17199–17204.
[9] S. Safaei, J. Wang, P.C. Junk, J. Solid State Chem. 294 (2021) 121762–121769.
[10] E. Moradi, R. Rahimi, Y.D. Farahani, V. Safarifard, J. Solid State Chem. 282 (2020) 121103–121111.
[11] Y.W. Zhao, Y. Wang, X.M. Zhang, ACS Appl. Mater. Interfaces 9 (2017) 20991–20999.
[12] Z.Q. Liu, Y.Q. Huang, W.Y. Sun, Inorg. Chem. 33 (2017) 1959–1969.
[13] X. Ma, K. Lu, B. Yuan, et al., Sens. Actuator. B: Chem. 369 (2022) 132373.
[14] L. van Pieterson, M.F. Reid, G.W. Burdick, A. Meijerink, Phys. Rev. B 65 (2002) 045114–045127.
[15] M. Kawa, J.M.J. Fréchet, Chem. Mater. 10 (1998) 286–296.
[16] M.D. Allendorf, C.A. Bauer, R.K. Bhakta, R.J.T. Houk, Chem. Soc. Rev. 38 (2009) 1330–1352.
[17] G.F. Ji, J.J. Liu, X.C. Gao, et al., J. Mater. Chem. A 5 (2017) 10200–10205.
[18] Y. Cue, F. Chen, X.B. Yin, Biosens. Bioelectron. 135 (2019) 208–215.
[19] J.L. Du, X.Y. Zhang, C.P. Li, et al., Sens. Actuator. B: Chem. 257 (2018) 207–213.
[20] K. Ren, S.H. Wu, X.F. Guo, H. Wang, Inorg. Chem. 58 (2019) 4223–4229.
[21] X. Zhang, Y. Yan, F.Q. Chen, et al., Z. Anorg. Allg. Chem. 647 (2021) 759–763.
[22] X.T. Zheng, A. Ananthanarayanan, K.Q. Luo, P. Chen, Small 11 (2015) 1620–1636.
[23] F. Copur, N. Bekar, E. Zor, S. Alpaydin, H. Bingol, Sens. Actuator. B: Chem. 279 (2019) 305–312.
[24] P.L. Gao, Z.G. Xie, M. Zheng, Chin. Chem. Lett. 33 (2022) 1659–1672.
[25] A. Lv, Q. Chen, C. Zhao, et al., Chin. Chem. Lett. 32 (2021) 3653–3664.
[26] S. Chandra, D. Bano, P. Pradhan, et al., Anal. Bioanal. Chem. 412 (2020) 3753–3763.
[27] P. Namdari, B. Negahdari, A. Eatemadi, Biomed. Pharmacother. 87 (2017) 209–222.
[28] R. Aggarwal, K. Bains, Crit. Rev. Food Sci. Nutr. 62 (2022) 2548–2559.
[29] W. Sun, C.X. Liu, Q.H. Chen, et al., Oxid. Med. Cell. Longev. 2018 (2018) 1–11.
[30] Y.H. Liu, M.J. Huang, P.Y. Wu, et al., Dalton Trans. 48 (2019) 13834–13840.
[31] H. Abd El-Wahab, M. Abd El-Fattah, A.H. Ahmed, A.A. Elhenawy, N.A. Alian, J. Organomet. Chem. 791 (2015) 99–106.
[32] X.L. Yang, C.J. Zhang, W.L. Dai, J.P. Liu, M.S. Wei, Chin. J. Catal. 33 (2012) 878–884.
[33] D.B. Wang, J.J. Liu, Z.L. Liu, J. Solid State Chem. 251 (2017) 243–247.
[34] T. Devic, C. Serre, N. Audebrand, et al., J. Am. Chem. Soc. 127 (2005) 12788–12789.
[35] L.F. Liu, Q. Hu, H.J. Sun, et al., J. Food Compost. Anal. 94 (2020) 103639–103647.
[36] M.J. Zhang, W.J. Ma, J.X. Cui, et al., J. Hazard. Mater. 383 (2020) 121152.
[37] Z.S. Han, K.Y. Wang, H. Min, et al., Angew. Chem. Int. Ed. 61 (2022) e202204066.
[38] Z.H. Chen, Y.L. Lu, L. Wang, et al., J. Am. Chem. Soc. 145 (2023) 260–267.
[39] Y.F. Guo, Z.S. Han, H. Min, et al., Small Struct. 3 (2022) 2100113.
[40] H. Min, S.Y. Wu, Z.S. Han, et al., Chem. Eur. J. 27 (2021) 17459–17464.
[41] Z.S. Han, K.Y. Wang, Y.L. Chen, et al., CCS Chem. 4 (2022) 3238–3245.
[42] L. Zhu, Y. Gu, G. Wu, J. Forest. Eng. 5 (2020) 97–102.
[43] W. Tan, X. Hao, Q. Wang, et al., J. Forest. Eng. 5 (2020) 97–103.
[44] W. Wei, Y. Li, Y. Li, et al., J. Forest. Eng. 5 (2020) 21–28.
[45] G. Chen, Y.Y. Yang, Q. Xu, et al., Nano Lett. 20 (2020) 8141–8150.
[46] M.X. He, L. Yu, Y.Y. Yang, et al., Chin. Chem. Lett. 31 (2020) 3178–3182.
[47] X.W. Li, W. Ma, D.H. Liang, et al., eScience 2 (2022) 646–654.
[48] X.K. Chen, X.D. Zhang, F.G. Wu, Chin. Chem. Lett. 32 (2021) 3048–3052.
[49] B. Ashok, N. Hariram, S. Siengchin, et al., J. Biores. Bioprod. 5 (2020) 180–185.
[50] C.D. Meng, S. Knežević, F.X. Du, et al., eScience 2 (2022) 591–605.
[51] K. Mizuno, S. Imafuji, T. Fujiwara, T. Ohta, Y. Tamiya, J. Phys. Chem. B 107 (2003) 3972–3978.
[52] M.N. Uddin, T. Ferdous, Z. Islam, et al., J. Biores. Bioprod. 5 (2020) 196–203.
[53] H. Yang, M.Q. Li, W.J. Zhao, et al., Chin. Chem. Lett. 32 (2021) 3882–3885.
[54] D.E. Ramírez-Herrera, A. Tirado-Guízar, F. Paraguay-Delgado, G. Pina-Luis, Microchim. Acta 184 (2017) 1997–2005.
[55] X.Z. Wang, X.R. Wang, Y.Y. Liu, et al., Ultrason. Sonochem. 59 (2019) 104734.
[56] T. Liu, Y.Y. Su, H.J. Song, Y. Lv, Analyst 138 (2013) 6558.
[57] S. Abbasi-Moayed, A. Bigdeli, M.R. Hormozi-Nezhad, ACS Appl. Mater. Interfaces 12 (2020) 52976–52982.
[58] T. Devic, V. Wagner, N. Guillou, et al., Microporous Mesoporous Mater. 140 (2011) 25–33.
[59] B. Ashok, N. Hariram, S. Siengchin, A.V. Rajulu, J. Biosci. Bioeng. 5 (2020) 180–185.
[60] M.N. Uddin, T. Ferdous, Z. Islam, et al., J. Biosci. Bioeng. 5 (2020) 196–203.
[61] W. Wei, Y. Li, Y. Li, et al., Forest Prod. J. 5 (2020) 21–28.
[62] L. He, T.T. Wang, J.P An, et al., CrystEngComm 16 (2014) 3259–3263.
[63] Y.Q. Zhou, Z.Z. Liu, G.M. Qiao, et al., Chin. Chem. Lett. 32 (2021) 3641–3645.
[64] Q.T. Xu, Z.H. Chen, H. Min, et al., Inorg. Chem. 59 (2020) 6729–6735.
[65] H. Min, Z.H. Chen, Z.S. Han, et al., Commun. Chem. 5 (2022) 74.
[66] Z.H. Chen, Z.S. Han, W. Shi, P. Cheng, Acta Chim. Sin. 78 (2020) 1336–1348.
[67] X.W. Li, C.Y. Liu, N. Gao, et al., Chin. Chem. Lett. 33 (2022) 2527–2531.
[68] Z.S. Han, W. Shi, P. Cheng, Chin. Chem. Lett. 29 (2018) 819–822.
[69] S.Y. Zhang, C.X. Yang, W. Shi, et al., Chem 3 (2017) 281–289.
[70] Z. Zhu, X. He, W.N. Wang, Catal. Sci. Technol. 22 (2020) 195–204.
[71] R. Wang, K.Q. Lu, Z.R. Tang, Y.J. Xu, J. Mater. 5 (2017) 3717–3734.
[72] L.J. Song, J.N. Xiao, R.X. Cui, et al., Sens. Actuator. B: Chem. 336 (2021) 129753.
[73] J.N. Xiao, M.Y. Liu, F.L. Tian, Z.L. Liu, Inorg. Chem. 60 (2021) 5282–5289.
[74] S. Jensen, K. Tan, W. Lustig, et al., J. Mater. Chem. C 7 (2019) 2625–2632.
[75] W. Shi, T.Z. Li, N. Chu, et al., Mater. Sci. Eng. C: Mater. 129 (2021) 112404.
[76] J. Zhang, H. Jia, W. Liu, J. Wang, D. Fang, Dyes Pigm. 193 (2021) 109554.
[77] H.R.H. Ali, A.I. Hassan, Y.F. Hassan, M.M. El-Wekil, J. Environ. Chem. Eng. 9 (2021) 105078.
[78] E. Domenichini, S. Doria, M. Di Donato, et al., Dyes Pigm. 174 (2020) 108010.
[79] G. Chen, M. Tang, X. Fu, et al., J. Mol. Struct. 1151 (2018) 235.
[80] I. Ahmed, H.J. Lee, S.H. Jhung, J. Mol. Liq. 344 (2021).
[81] J.N. Xiao, L.J. Song, M.Y. Liu, X.L. Wang, Z.L. Liu, Inorg. Chem. 59 (2020) 6390–6397.
[82] R.X. Cui, Y.Y. Wan, G.F. Ji, Z.L. Liu, Analyst 144 (2019) 5875–5881.